# SUPPORTING INFORMATION

# Phase-tuned layered 1T W-$MoS_2$/PEDOT:PSS hybrid: Functional engineering towards self-binding supercapacitor cathode

*Chandru Gunasekaran[a], Ganesan Shanmugam*[a] and Sachin Sreedhar[a]*

[a] Energy Conversion and Energy Storage Laboratory, Department of Chemistry, SRM Institute of Science and Technology, Kattankulathur, Tamil Nadu - 603 203, India.

*Corresponding author e-mail: sakthi_ganesan@rediffmail.com, ganesans2@srmist.edu.in

## Table of Content

## Instrumental Analyses

The crystallographic analysis of pristine and hybrids was conducted using Powder X-ray diffraction (P-XRD) with BRUKER USA D8 Advance Davinci Diffractometer with Cu Ka radiation with 2θ range from 10° to 80°. The degree of defects in materials was observed by micro-Raman spectrometer using HORIBA, Lab Ram HR Evolution. The surface morphology and elemental compositions were characterised using a High-resolution Scanning Electron Microscope (HR-SEM) (Thermo Scientific Apero S) and High-resolution Transmission Electron Microscope (HR-TEM) (JEM-2100 Plus). HR-TEM was also utilized to capture Energy Dispersive X-ray Spectroscopy (EDS) images. X-ray Photoelectron Spectroscopy (XPS) was employed to determine the element composition and valance state in the pristine $MoS_2$ and 10W-MS/P hybrid materials. The Brunauer-Emmett-Teller (BET) method was used to measure the pore volume and specific surface area of the 10W-MS/P hybrid material (Quantachrome Instruments, Autosorb IQ series). Finally, Thermogravimetric Analysis (TGA) was conducted to evaluate the thermal stability of the pristine $MoS_2$ and 10W-MS/P hybrid materials.

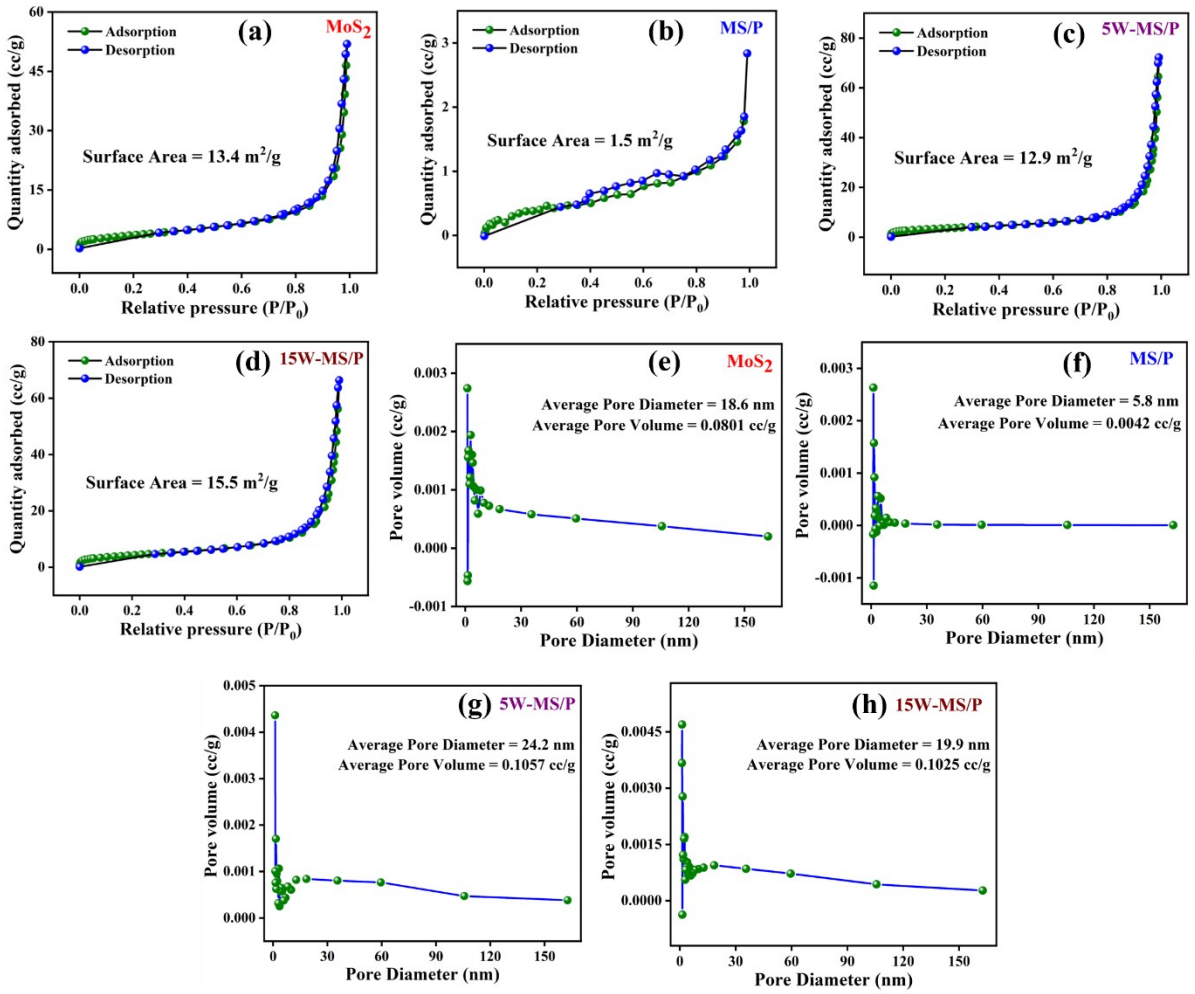


**Fig. S1.** N2 adsorption-desorption curves of a) $MoS_2$, b) MS/P, c) 5W-MS/P, d) 15W-MS/P, and pore size distribution curve of e) $MoS_2$, f) MS/P, g) 5W-MS/P, h) 15W-MS/P.

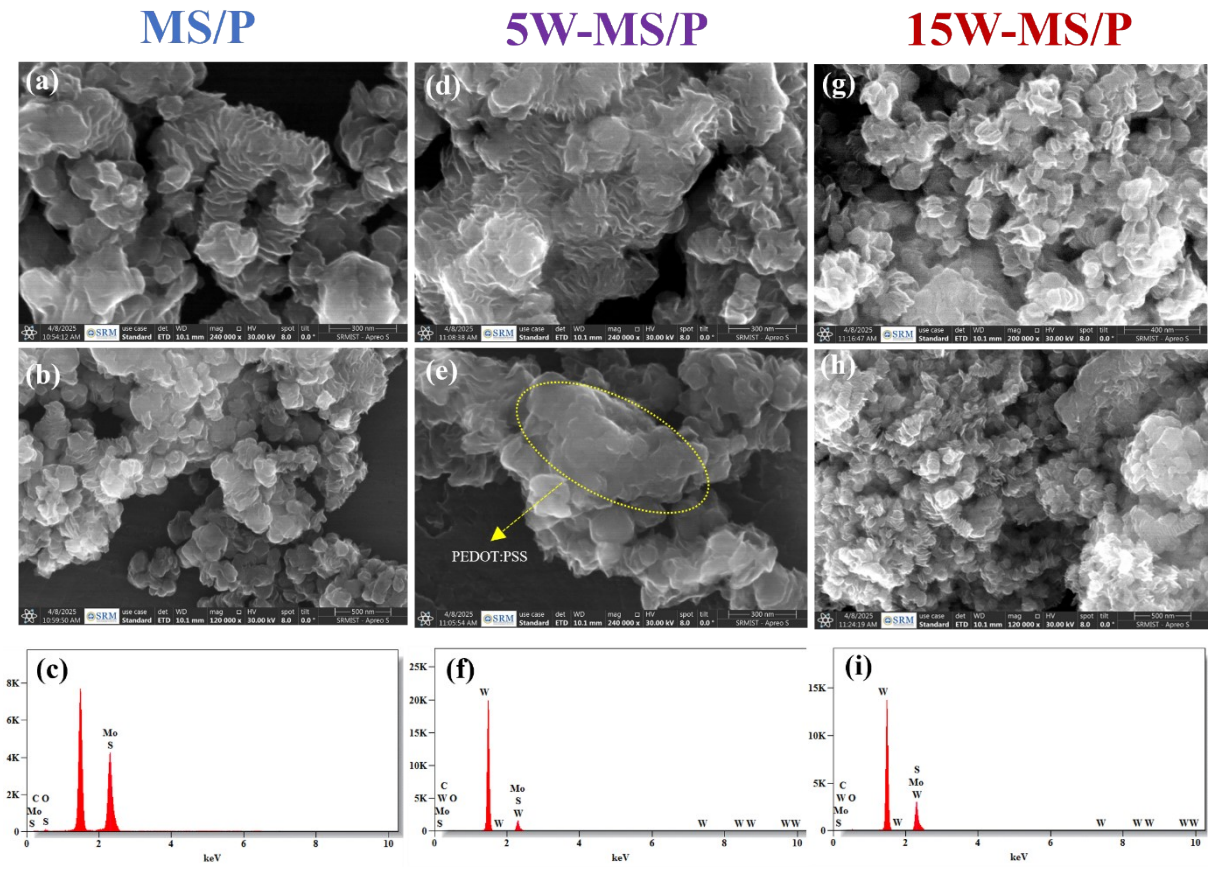


**Fig. S2.** HR-SEM images and EDX Spectra of a) – c) MS/P hybrid, d) – f) 5W-MS/P hybrid, and g) – i) 15W-MS/P hybrid.

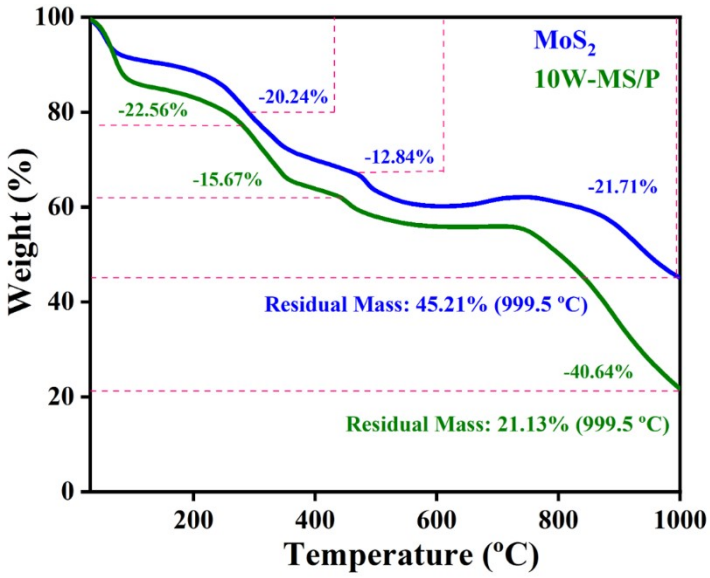


**Fig. S3.** TGA analysis of $MoS_2$ and 10W-MS/P.

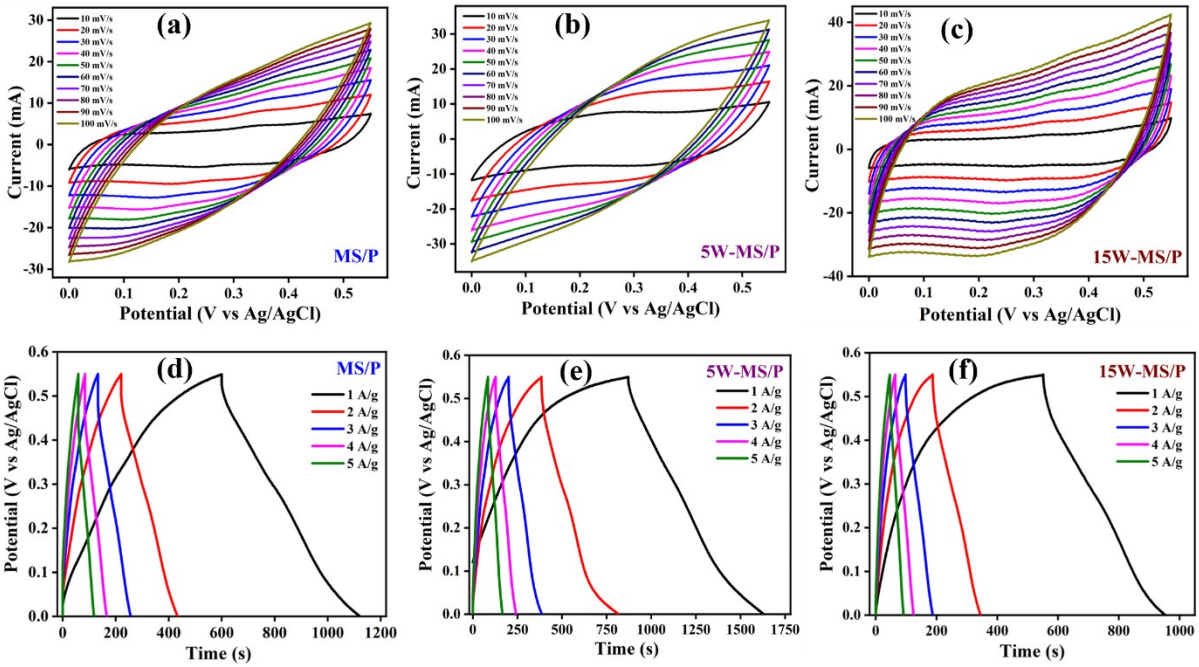


**Fig. S4.** CV curves of a) MS/P, b) 5W-MS/P, c) 15W-MS/P, and GCD curves of d) MS/P, e) 5W-MS/P, and f) 15W-MS/P.

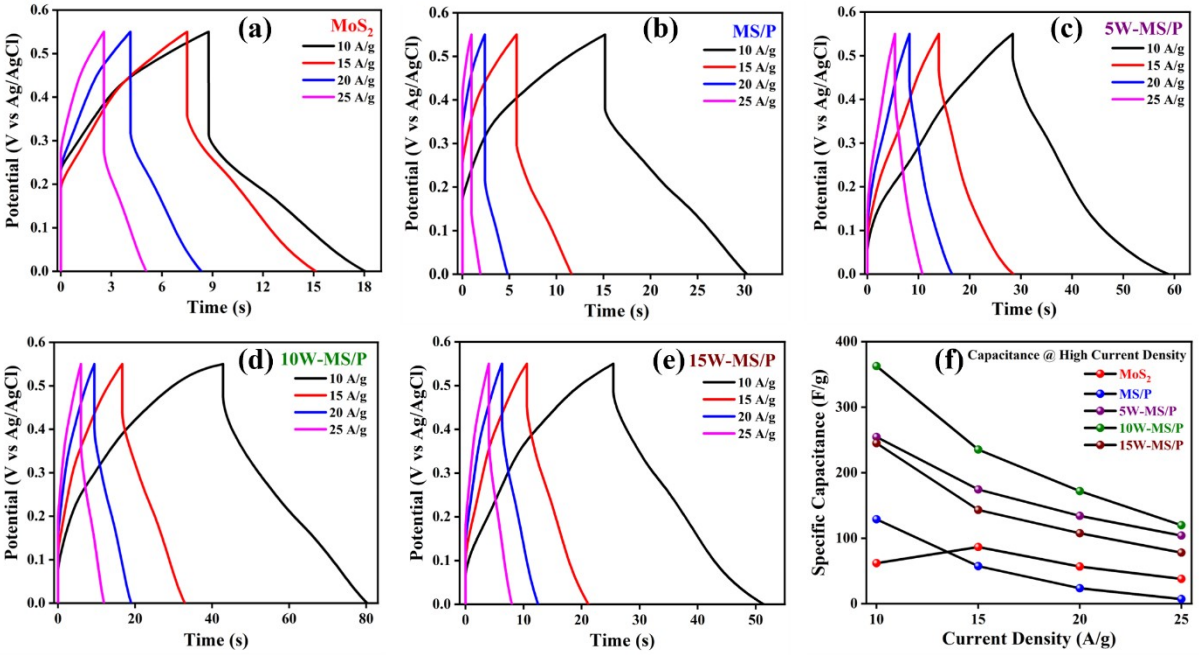


**Fig. S5.** GCD curves of a) $MoS_2$, b) MS/P, c) 5W-MS/P, d) 10W-MS/P, e) 15W-MS/P, and f) specific capacitance at higher current densities.

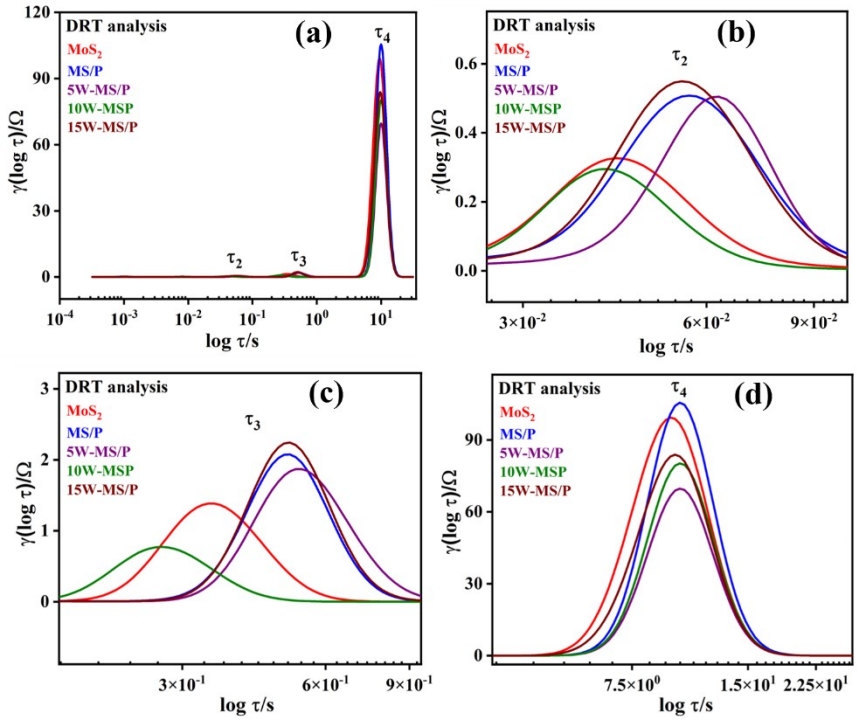


**Fig. S6.** a) Distribution of Relaxation Time (DRT) analysis, b) charge-transfer resistance ($R_{ct}$), c) interfacial polarization/electric double layer capacitance ($C_{dl}$), and d) diffusion related contributions of $MoS_2$, MS/P, 5W-MS/P, 10W-MS/P, and 15W-MS/P.

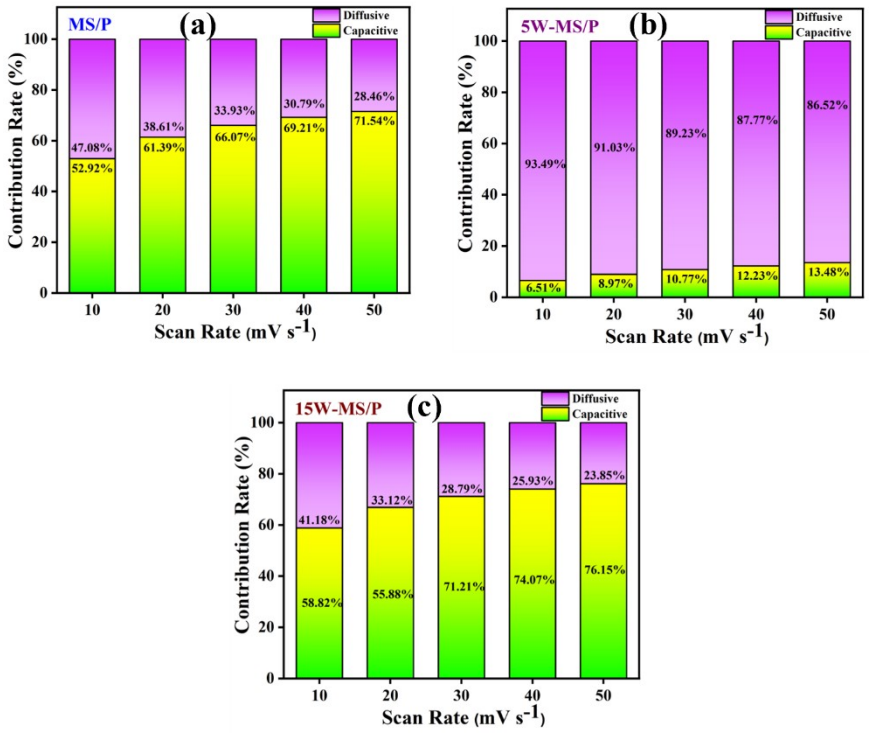


**Fig. S7.** Contribution bar graph of a) MS/P, b) 5W-MS/P, and c) 15W-MS/P.

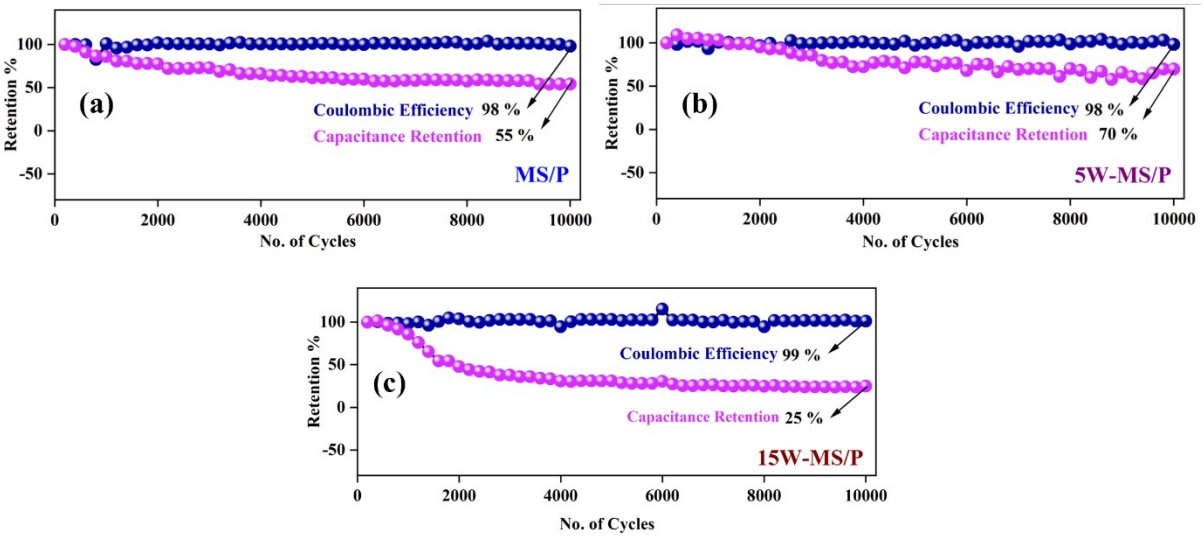


**Fig. S8.** Cyclic stability at 15 A/g over 10,000 cycles of a) MS/P, b) 5W-MS/P, and c) 15W-MS/P.

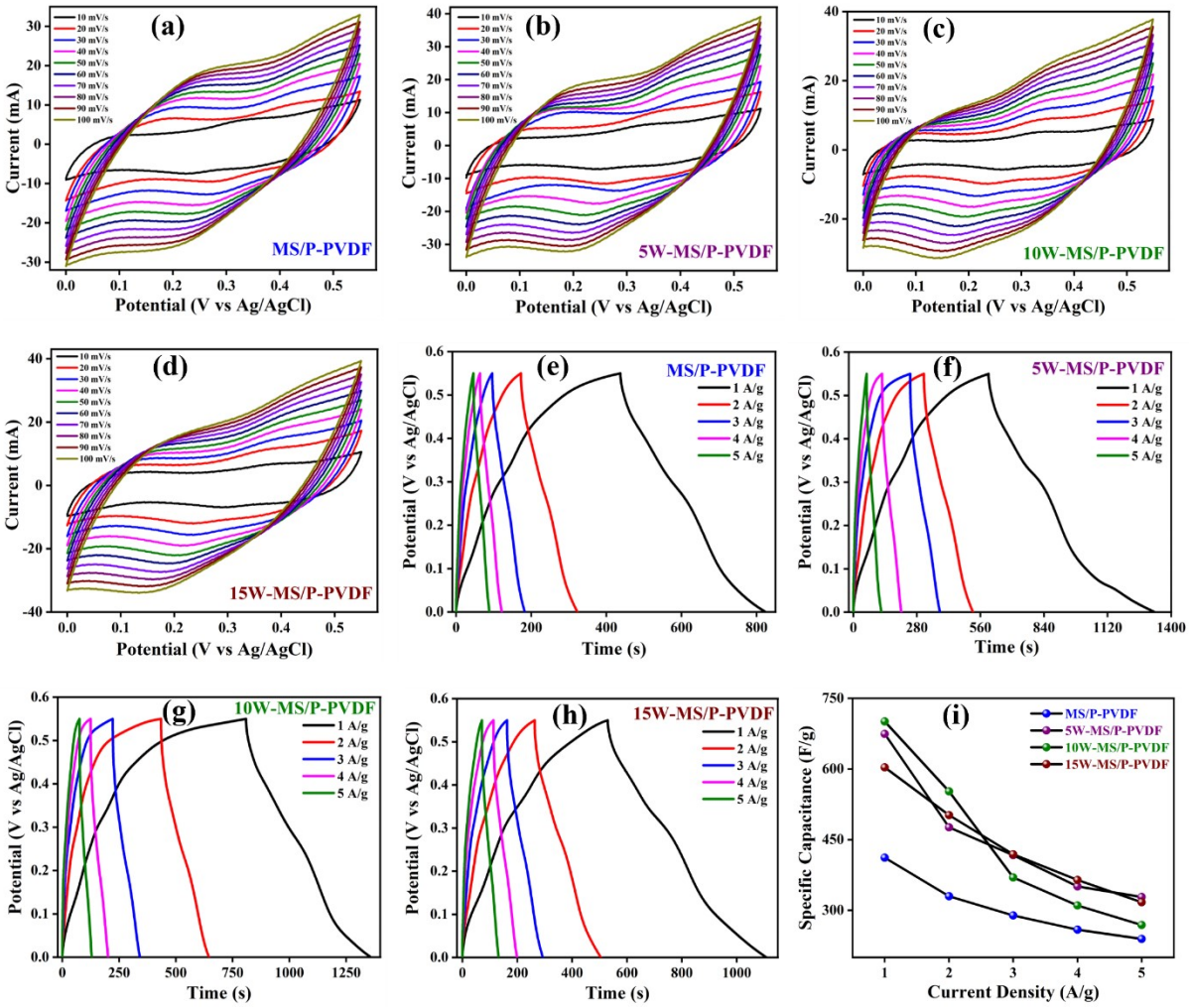


**Fig. S9.** a) – d) CV curves, e) – f) GCD curves, and i) specific capacitance at higher current densities for MS/P-PVDF, 5W-MS/P-PVDF, 10W-MS/P-PVDF, and 15W-MS/P-PVDF.

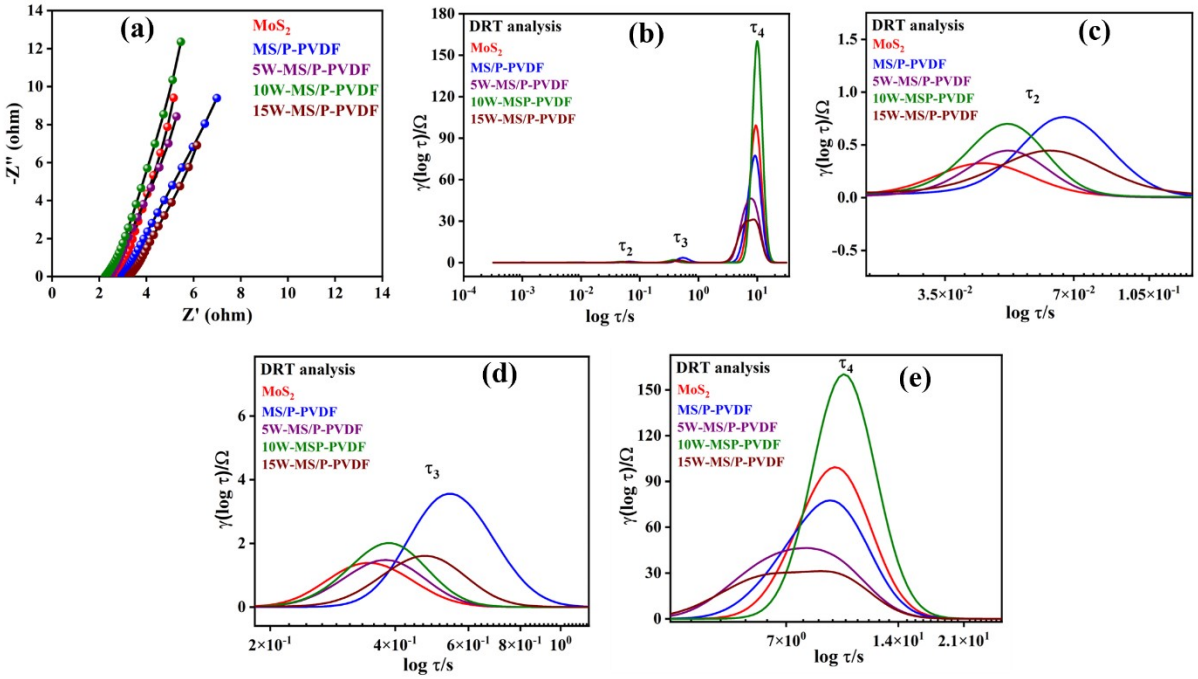


**Fig. S10**. a) EIS, b) Distribution of Relaxation Time (DRT) analysis, c) charge-transfer resistance ($R_{ct}$), d) interfacial polarization/electric double layer capacitance ($C_{dl}$), and e) diffusion related contributions for MS/P-PVDF, 5W-MS/P-PVDF, 10W-MS/P-PVDF, and 15W-MS/P-PVDF.

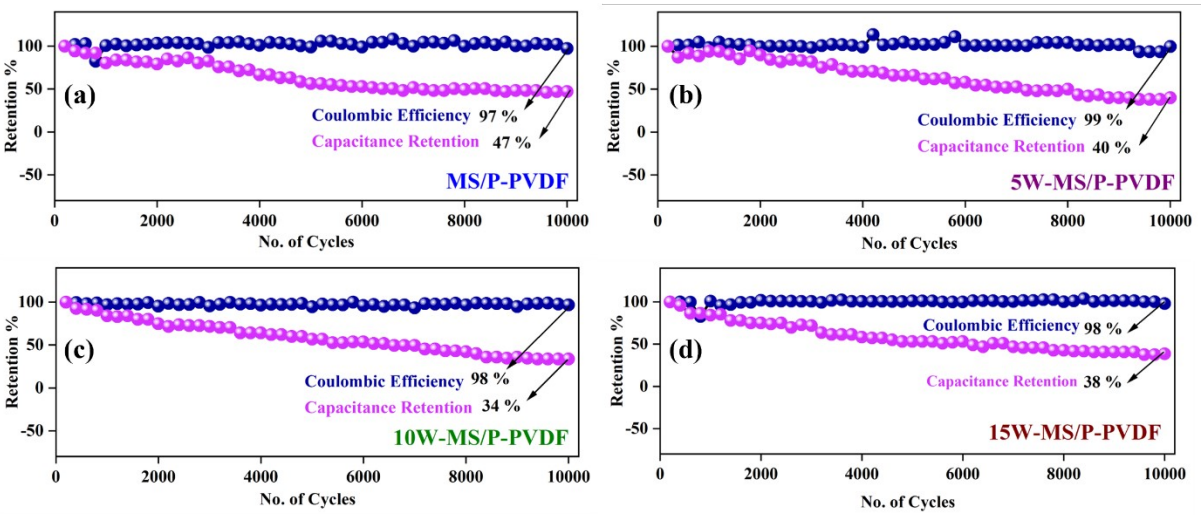


**Fig. S11.** Cyclic stability at 15 A/g over 10,000 cycles of a) MS/P-PVDF, b) 5W-MS/P-PVDF, c) 10W-MS/P-PVDF, and d) 15W-MS/P-PVDF.

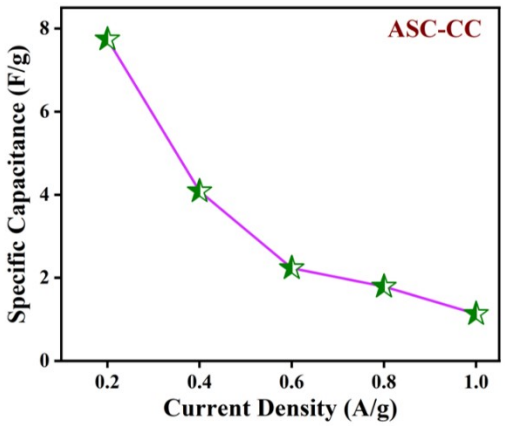


**Fig. S12.** Specific capacitance of ASC-CC device at various current densities.

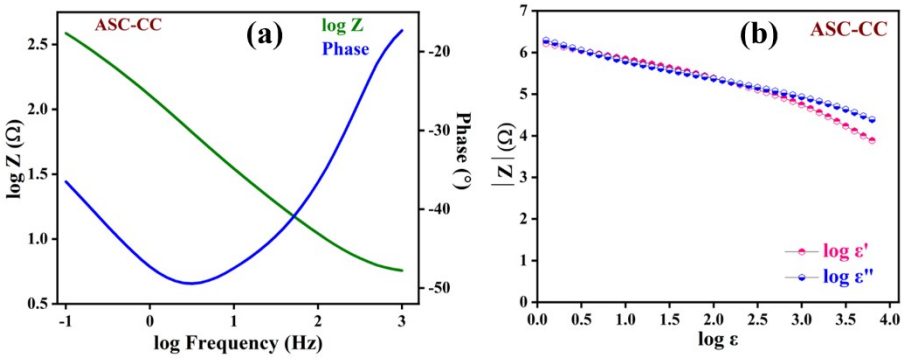


**Fig. S13.** a) Bode plot of the device, and b) dielectric constant and dielectric loss.

**Table S1:** Comparative analysis of electrochemical performance of the $MoS_2$ based materials.

| *S. No* | *Material* | *Electrolyte* | *Specific Capacitance* | *Cyclic performance* | *Ref.* |
|---|---|---|---|---|---|
| ***1*** | Ni-$MoS_2$ | 1 M $Na_2SO_4$ | 425 F/g | 10,000 (60%) | [1] |
| ***2*** | PPy/PANI@$MoS_2$ | 1 M $H_2SO_4$ | 1171 F/g | 6,000 (89%) | [2] |
| ***3*** | Poly (3,4-ethylenedioxythiophene) Nanocomposite | 1 M $H_2SO_4$ | 90 F/g | 15,000 (93%) | [3] |
| ***4*** | 1T-$MoS_2$@$Ti_3C_2T_x$ | 1 M $H_2SO_4$ | 425 F/g | 20,000 (91.2%) | [4] |
| ***5*** | $MoS_2$@PANI | 1 M $NH_4Cl$ | 450 F/g | 5,000 (86.3%) | [5] |
| ***6*** | 2H-$MoS_2$/MXene | 1 M $(NH_4)_2SO_4$ | 722.13 F/g | 5,000 (90.1%) | [6] |
| ***7*** | $MnMoO_4$@$MoS_2$ | 1 M KOH | 319 F/g | 10,000 (87.9%) | [7] |
| ***8*** | $Sb_2S_3$/$MoS_2$ | 1 M $(NH_4)_2SO_4$ | 360 F/g | 5,000 (90%) | [8] |
| ***9*** | $M_xMo_{1-x}S_2$/C Nanohybrids | 1 M KOH | 184 F/g | 1,000 (82%) | [9] |
| ***10*** | **1T $W_{0.1}$-$Mo_{0.9}S_2$/PEDOT:PSS** | **1 M $H_2SO_4$** | **845.14 F/g** | **10,000 (89%)** | **This Work** |

*PEDOT - Poly (3,4-ethylenedioxythiophene)*

*PSS - Polystyrene sulfonate*

*PPY - Polypyrrole*

*PANI - Polyaniline*

## References


1 S. J. Panchu, K. Raju, P. Singh, D. D. Johnson and H. C. Swart, *ACS Appl. Energy Mater.*, 2023, **6**, 2187–2198.

2 L. Luo, X. Wang, S. Yang, J. Dai, D. Li, L. Xia, C. Chi, A. Cabot, Y. Xu and L. Dai, *ACS Appl. Energy Mater.*, 2023, **6**, 5940–5951.

3 Z. Wang, P. Tammela, J. Huo, P. Zhang, M. Strømme and L. Nyholm, *J. Mater. Chem. A Mater.*, 2016, **4**, 1714–1722.

4 S. Ye, Y. Zhang, C. An, S. Xiang and G. Wu, *Adv. Funct. Mater.*, 2025, **35**, 2419779.

5 J. Dai, C. Yang, Y. Xu, X. Wang, S. Yang, D. Li, L. Luo, L. Xia, J. Li and X. Qi, *Advanced Materials*, 2023, **35**, 2303732.

6 X. Zhang, Z. Wang, J. Luo, S. Ali, Y. Xie, Y. Zhao, P. Lu, M. S. Javed, A. Ahmad and A. M. Tighezza, *Small*, 2025, **21**, e05627.

7 A. V. A, A. Singh, N. Tripathy, P. Lakhiwal, M. Iqbal, R. Kumar, M. K. Kashyap, A. De Sarkar and S. K. Mahapatra, *Adv. Funct. Mater.*, 2025, **35**, 2421379.

8 S. J. Marje, H. B. Tyagaraj, S.-K. Hwang, K. S. Ranjith, E. Alhajri, N. R. Chodankar, Y. S. Huh and Y.-K. Han, *J. Mater. Chem. A Mater.*, 2024, **12**, 7587–7597.

9 S. Yao, S. Zhang, G. Zhang, Y. Tang, R. Zhu, Y. Peng, Y. Chen and H. Pang, *Inorg. Chem.*, 2023, **62**, 16038–16046.